

# Magnetically tuned, robust and efficient filtering system for spatially multimode quantum memory in warm atomic vapors

Michał Dąbrowski, Radosław Chrapkiewicz\*, and Wojciech Wasilewski\*

Warm atomic vapor quantum memories are simple and robust, yet suffer from a number of parasitic processes which produce excess noise. For operating in a single-photon regime precise filtering of the output light is essential. Here we report a combination of magnetically tuned absorption and Faraday filters, both light-direction-insensitive, which stop the driving lasers and attenuate spurious fluorescence and four-wave mixing while transmitting narrowband Stokes and anti-Stokes photons generated in write-in and readout processes. We characterize both filters with respect to adjustable working parameters. We demonstrate a significant increase in the signal to noise ratio upon applying the filters seen qualitatively in measurements of correlation between the Raman-scattered photons.

## I. INTRODUCTION

Quantum memories are the essential building-blocks in a number of quantum information processing protocols [1]. Examples include building a quantum network connecting space-separated atomic memories via optical fibers [2], quantum computation [3, 4], quantum communication [5], entanglement [6] and multiple-photon generation on demand [7].

A number of different implementations of quantum memory have been realized so far including electromagnetically induced transparency [8], Raman scattering [9], atomic frequency comb [10, 11], gradient echo memory [12] and coherent population oscillations [13]. Among the most popular media for storage of the quantum information are cold alkaline atoms [14–17], room-temperature atomic vapors in cells [9, 18–21] and in hollow-core fibers [22, 23], molecular gases [4, 24], NV-centres [25] and optical phonons [6] in diamonds, and rare-earth-doped solids [26, 27].

In this work we focus on probably the most widespread and renowned implementation based on warm alkali atom vapor (rubidium-87) contained in a glass cell together with noble buffer gas (krypton) to reduce the effects of thermal motion [28, 29]. Photons are interfaced with atomic collective excitations, spin-waves, via off-resonant Raman transitions. We operate on memory in spatially multimode regime using large diameter driving beams [30]. In general multimode operation is natural and readily achievable in a number of spontaneous and parametric processes [31–33] such as spontaneous parametric down-conversion in non-linear crystals [34] and instantaneous four-wave mixing in warm atomic vapors [35, 36]. In our application spatially multimode operational mode can be applied to store transversely varying information, such as images, in quantum memories [20, 37, 38]. In our setup typically over one hundred distinguishable spatial modes of Raman light are coupled with independent spin-wave modes [39].

Spontaneous Raman scattering in warm and high optical depth ensembles is most efficient at the detuning of the order of 1 GHz and requires significant drive

laser energy. Thus filtering out of the driving beams requires very large attenuation, around  $10^{11}$ . In our experiments first we use crystal polarizers, as the Raman photons are polarized orthogonally to the driving light. Next a rubidium-85 absorption filter [17, 40] of magnetically broadened absorption line width is used to stop any remaining leakage. The second type of noise is an omnidirectional spontaneous fluorescence directly from the excited state, observed in a number of experiments [21, 41, 42] and discussed theoretically [43–46]. This fluorescence is enhanced by collisions with buffer gas [4, 41, 42]. Our experiments also indicate presence of broadband and omnidirectional noise light of an intensity proportional both to the concentration of Rubidium and the buffer gas, likely due to the scattering of laser light by the long-lived Rb-buffer gas molecules [47].

To filter out this light, a narrow bandpass filter transmitting the Raman light only is necessary. Typically a Fabry-Perot cavity is used to this end [5, 21, 42]. However, it is unsuitable for our purposes, because it cannot transmit hundreds of spatial modes at the same frequency. Therefore we use a Faraday filter [48, 49] with

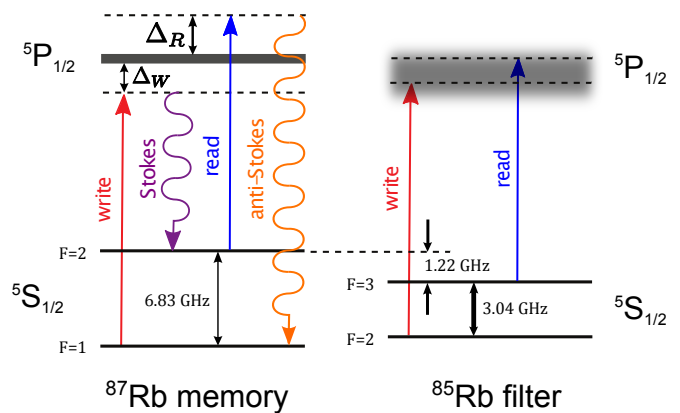


Figure 1. Driving lasers and photons frequencies against rubidium-87 and rubidium-85 energy level structure. Write and read lasers are virtually resonant with Doppler- and magnetically broadened  $^{85}\text{Rb}$  isotope transitions in absorption filter as opposed to scattered photons.

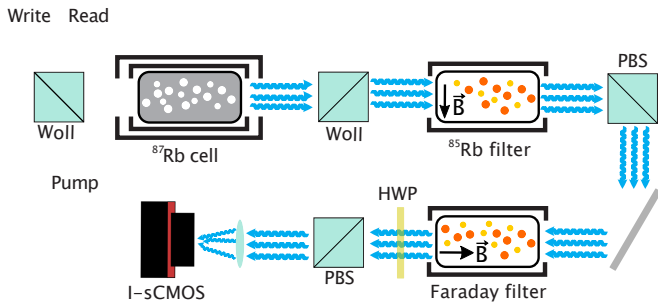


Figure 2. Experimental setup of quantum memory and filters system. From top-left corner:  $^{87}\text{Rb}$  atomic memory cell inside magnetic shielding, magnetically broadened  $^{85}\text{Rb}$  absorption filter, Faraday filter and a low-noise, single-photon-sensitive intensified sCMOS camera (I-sCMOS) as a detector. The blue squares stand for polarizing beam splitter cubes (PBS) or Wollaston polarizers (Woll). The directions of the magnetic field are marked.

rubidium-87 vapor rotator as a second stage. By properly adjusting the temperature and magnetic field in both filters we are able to attenuate the driving beams by a factor of  $10^{11}$  and reach a transmission of 65% for the Stokes and 45% for the anti-Stokes light.

We demonstrate the immense effect of combined filtering on the statistical properties of the registered light. The first filter virtually stops the driving laser leakage. However, only due to the application of the second filter intensity correlations between the Stokes and anti-Stokes scattered light can be seen down to a single-photon level. The approach we demonstrate is a robust alternative to filtering with the use of interference cavities. It is insensitive to direction and precise alignment although its tuning is possible just through adjusting the magnetic field and temperature in both filters.

## II. MEMORY SETUP

In our experiments we start with an ensemble of  $^{87}\text{Rb}$  atoms pumped to  $F=1$  state. We write to the memory by driving spontaneous Stokes transition, which produces pairs of collective excitations to the  $F=2$  state, i.e. spin-waves and scattered Stokes photons. After adjustable storage time the spin-wave can be converted to anti-Stokes photons by sending read laser pulse [5, 20, 50]. Both drive lasers work near D1-line transitions. The detunings of write and read lasers from resonances  $F = 1 \rightarrow F' = 1$  and  $F = 2 \rightarrow F' = 2$  equal  $\Delta_W = 1$  GHz and  $\Delta_R = 800$  MHz respectively as indicated in Fig.1.

The simplified version of the experimental setup is depicted in Fig. 2. We utilize three external cavity diode lasers (ECDL) for optical pumping and Raman scattering in the  $^{87}\text{Rb}$  cell. The Raman scattered light has a polarization orthogonal to the driving lasers, so we use Wollas-

ton prisms to pre-filter the Raman-scattered light. Due to the finite extinction of the Wollaston prisms ( $10^3:1$ ) a small portion of laser light leaks together with the Raman-scattered light. Usage of the  $^{85}\text{Rb}$  leads to a high absorption coefficient of the driving lasers whereas transmission of Raman-scattered light remains at the level of 80%. Properties of the atomic absorption filter are independent of the transmitting light properties, e.g. direction, spatial mode profile or polarization, in contrast to the properties of the Faraday or Voigt filters. Finally, the broadband light coming from the resonant fluorescence is filtered out with the use of the Faraday filter. This filter additionally diminishes the residual leakage of driving beams.

The photons are detected with a high-resolution sCMOS camera with an image intensifier (I-sCMOS) [51–53, 55]. This enables us to work in a single-photon-level regime and to measure photon statistics in a similar manner as with multiplexed on-off detectors [51, 53–55]. Further details of the experimental setup and the full operational scheme of our quantum memory protocol are described in [20, 50].

Absorption and transmission spectra of the three rubidium cells used in the experiment are presented in Fig. 3 along with the positions of the laser beams frequencies, as well as Stokes and anti-Stokes scattered light. Detuning of about 1 GHz for both write-in and readout beams is a compromise between the high efficiency of Raman scattering and the low absorption coefficient inside the filtering cells.

## III. FILTERING SYSTEM - DETAILS

### A. Absorption filter

The 30-cm long rubidium  $^{85}\text{Rb}$  cell in the transverse static magnetic field, drawn in Fig. 4, is used to stop the strong laser beams and transmit the Raman-scattered single photons which are very narrowband but their frequencies lie out of the wings region of the spectrum. The transverse magnetic field inside the filter is emitted by the ferrite magnets located on both sides of the rubidium cell. By changing the distance between the magnets, we effectively change the magnetic field inside the cell and thence the line broadening. The width of the absorption spectrum controlled by the magnetic field ranges from 5.5 GHz up to 8.4 GHz, depending on the distance between the magnets, as depicted in Fig. 5. For our purposes we set the magnetic field to  $10^{-2}$  T for a 9-cm distance between magnets, to move  $^{85}\text{Rb}$  lines close enough to  $^{87}\text{Rb}$  where driving lasers operate.

The opaqueness and to some extent the temperature of the filter lines are tuned by changing the temperature of the filter. The filter is heated in a range of  $20^\circ - 140^\circ$  C to vary the optical density of atomic vapor that grows

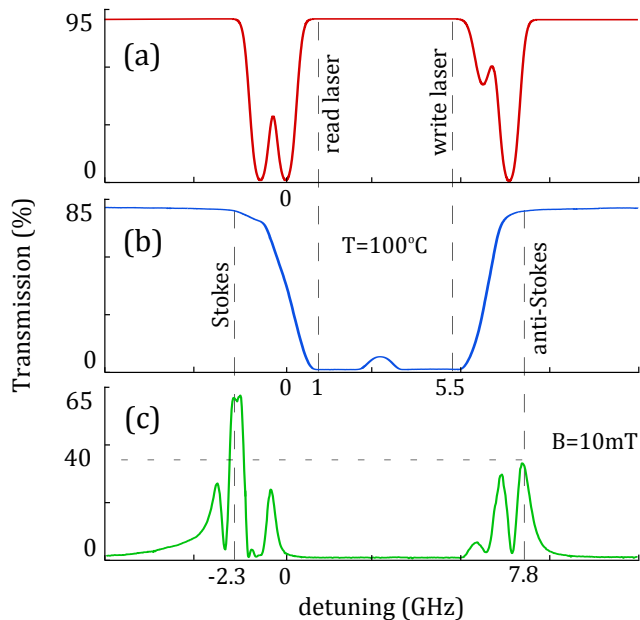


Figure 3. Transmission spectra of (a) the atomic quantum memory cell containing  $^{87}\text{Rb}$  isotope, (b)  $^{85}\text{Rb}$  absorption filter at  $T = 100^\circ\text{C}$  and (c)  $^{87}\text{Rb}$  Faraday filter for the magnetic field amplitude  $B = 10^{-3}$  T and temperature  $T = 102^\circ\text{C}$ . The frequency of the laser beams and scattered Stokes and anti-Stokes light are marked by detunings measured from  $F = 2 \rightarrow F' = 2$  transition on D1-line in  $^{87}\text{Rb}$ .

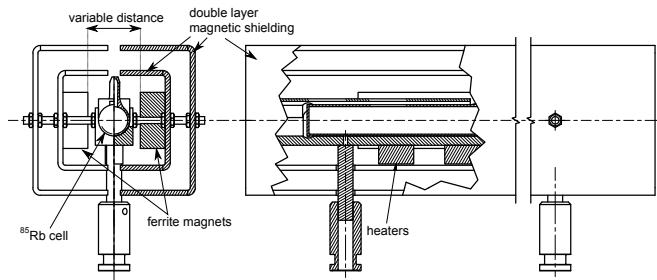


Figure 4. Technical drawing of the magnetically tuned absorption filter based on  $^{85}\text{Rb}$  isotope. Broadening of filter lines is achieved by changing a variable distance between ferrite magnets. Filter is embedded in a two-layer magnetic shielding protecting main quantum memory cell from the corrupting stray magnetic field.

exponentially with temperature. In practice the operational range is limited, as for temperatures below  $90^\circ\text{C}$  the absorption of drive lasers is too low while above  $120^\circ\text{C}$  the transmission of the Raman-scattered light drops abruptly.

The whole filter is inserted inside the two-layer soft-steel magnetic shielding that confines the magnetic field inside the filter suppressing the stray external fields down to  $B_{ext} \simeq 10^{-4}$  T. We heat the vapors in the Rubidium cell using the high-power resistor mounted under the cell which dissipates around  $P \simeq 80$  W power.

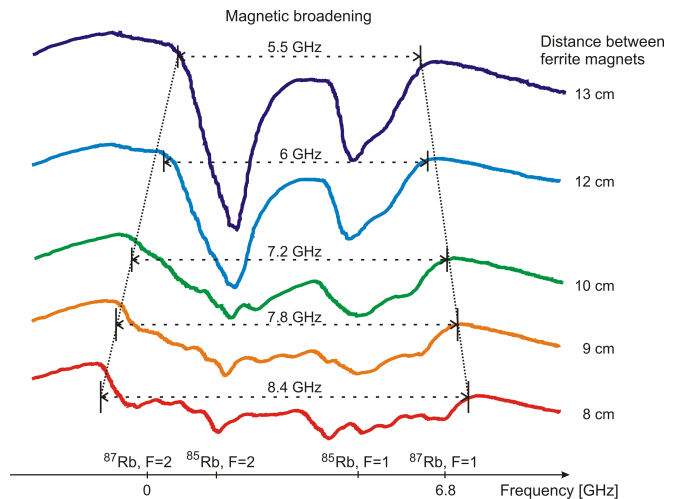


Figure 5. Large broadening of the lines of absorption filter due to transverse magnetic field, tuned by changing distance between ferrite magnets. For visualization purposes presented transmission spectra were measured below operation temperature, at  $T = 60^\circ\text{C}$ . For our operation we selected a distance of 9 cm corresponding to  $10^{-2}$  T inside the cell with  $^{85}\text{Rb}$ . Spectra are juxtaposed vertically, with proportions preserved.

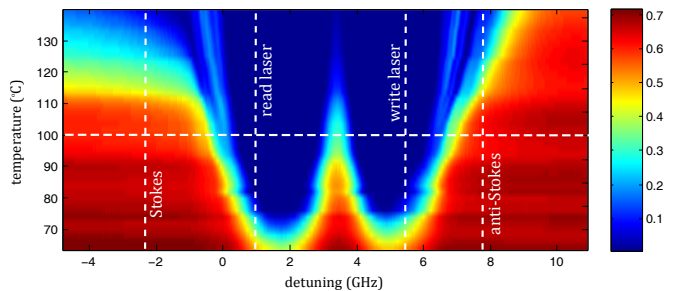


Figure 6.  $^{85}\text{Rb}$  filter transmission spectra for a range of temperatures. Absorption lines are significantly broadened due to transverse magnetic field of approximately  $10^{-2}$  T. The detuning is measured from  $F = 2 \rightarrow F' = 2$  transition on the D1-line of  $^{87}\text{Rb}$ .

Measured transmission spectra for different temperatures in the frequency range of both lasers and the scattered light are shown in Fig. 6. For large positive detunings the wing of the spectrum transmission is smaller than for negative detunings due to the residual content of  $^{87}\text{Rb}$  in the filter cell. For optimal temperature  $T_{abs} = 100^\circ\text{C}$  the suppression of the drive lasers is 50 dB while the transmission of the Raman-scattered light is at the level of 80%. The frequencies of Stokes and anti-Stokes scattered light in Fig. 6 correspond to detunings  $\Delta_S = -2.3$  GHz and  $\Delta_{AS} = 7.8$  GHz, respectively.

## B. Faraday filter

To filter out the broadband fluorescence and four-wave mixing accompanying write-in and readout from the memory, we utilize a Faraday filter which consists of two orthogonal polarizers and a Faraday rotator in between. In this arrangement the filter is opaque in the absence of magnetic field. We use the standard configuration of the filter [48, 56], but for temperature stabilization purposes we apply water cooling to compensate the relatively high power emitted by coils producing magnetic field.

The rotation of the polarization occurs in a 30-cm long cell containing the  $^{87}\text{Rb}$  isotope heated up to  $100^\circ\text{C}$  for us to obtain appropriate optical density of vapors. The magnetic field inside the filter is about  $B = 10^{-2}\text{ T}$  and directed along the beam. The average magnetic field does not depend on the transverse position inside the cell, i.e. it is near perfectly uniform in each plane perpendicular to the laser beam direction. The imperfections of the magnetic field in the transverse directions are smaller than  $10^{-5}\text{ T}$ . The cell is placed in a PVC tube and heated with a current flowing through the coils wound around the  $^{87}\text{Rb}$  glass cell. Other coils outside the PVC tube produce strong magnetic field along the filter axis. The filter is inside a soft-steel pipe with lids to contain the magnetic field inside the filter. The whole system is additionally sealed in another, outer pipe, where circulating water transfers out the heat emitted by the coils.

The transmission through the system with two orthogonal polarizers and the rotator between reads  $t = t_{rot} \sin^2 \theta$ , where  $t_{rot}$  is the transmission through the rotator and  $\theta$  is the rotation angle. To elucidate the above expression, consider the linearly polarized light entering the rotator decomposed in a left (L) and right (R) circular polarization basis. Each of them has a refractive index  $n_{L,R}$  and an absorption coefficient  $\alpha_{L,R}$ . Traveling through the rotator each circular polarization acquires a phase  $\exp(iK_{L,R}z)$ , where  $K_{L,R} = n_{L,R}\omega/c + i\alpha_{L,R}z$  is the complex wavevector. The resulting rotation angle due to the difference between refractive indices equals  $\theta = (n_L - n_R)\omega/2c$ . For the sake of simplicity we assume equal absorption coefficients for both circular polarization components  $\alpha_L \simeq \alpha_R = \alpha$ , yielding the expression for the total transmission  $t_{rot} = \exp(-\alpha z)$ .

The transmittance spectrum of the Faraday filter with two orthogonal polarizers is presented in Fig. 7 for the whole spectrum of rubidium-87 D1-line. The transmission spectrum is measured for different values of the external magnetic field at the temperature of  $T = 68^\circ\text{C}$ . For very weak magnetic fields there is almost no transmission while in strong magnetic fields numerous separate high-transmission bands emerge. They correspond to rotation angles  $\theta = \pi + 2\pi k$ , where  $k$  stands for an integer number.

Fig. 8 presents analogous spectra but measured in a

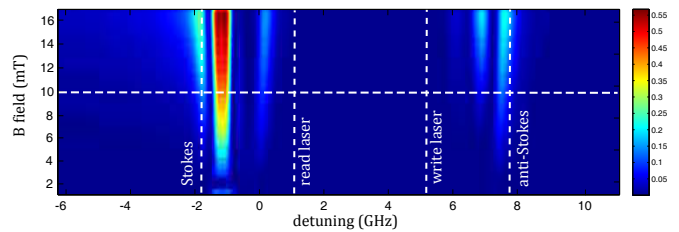
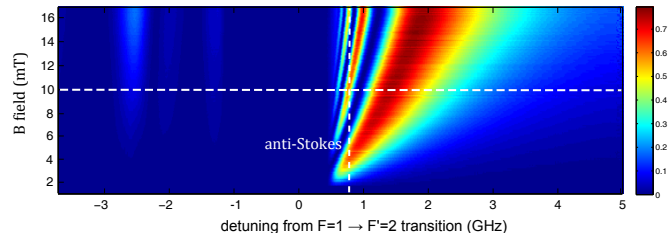
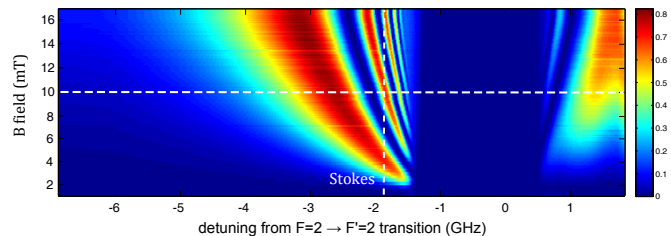


Figure 7. Transmission spectra of the Faraday filter at  $T = 68^\circ\text{C}$  for different values of magnetic field. The detuning is measured from  $F = 2 \rightarrow F' = 2$  transition on the D1 line of  $^{87}\text{Rb}$ .



(a) Part of Rb spectrum in the region of  $F=1$  ground-state sublevel transition.



(b) Part of Rb spectrum in the region of  $F=2$  ground-state sublevel transition.

Figure 8. Transmission spectra of the Faraday filter with a hot cell at  $T = 110^\circ\text{C}$  for different values of magnetic field zoomed to the vicinity of the  $^{87}\text{Rb}$  resonances.

detailed frequency scale at a higher temperature  $T = 110^\circ\text{C}$ , separately for the two different regions of the D1 line of Rubidium: near the the  $F = 1 \rightarrow F' = 2$  and  $F = 2 \rightarrow F' = 2$  transitions, respectively. Fig. 9 compares two relative orientations of polarizers parallel and perpendicular to each other at  $T = 90^\circ\text{C}$ .

For the perpendicular polarizers the transmission  $t_{\perp} = t_{rot} \sin^2 \theta$  reaches its maximum for a rotation angle  $\theta = \pi + 2\pi k$  provided the transmission through rotator  $t_{rot}$  is nonzero. Although in the vicinity of the resonance the rotation may be high, the rotator becomes opaque [48]. On the other hand, further away from the resonances the net polarization rotation is very small, since both circular polarization components are subject to virtually the same retardation. Increase in the magnetic field pushes the transmission line further from the resonances. Practically the filter transmits frequencies detuned by 1-3 GHz from any of the four resonances of  $^{87}\text{Rb}$  D1 line, depicted in Fig. 3 (a).

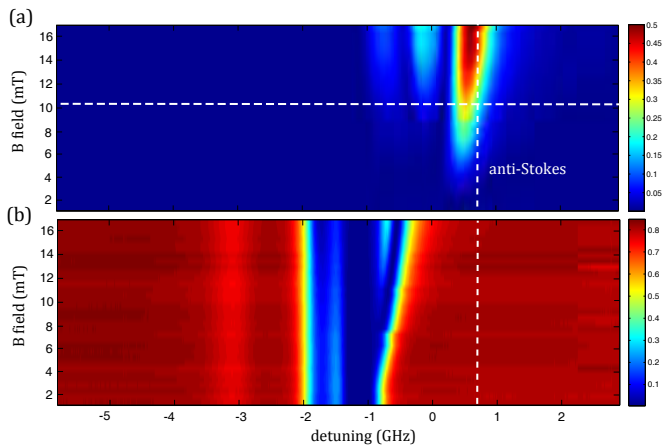


Figure 9. Transmission spectra of the Faraday filter at  $T = 90^\circ \text{C}$  with (a) perpendicular and (b) parallel polarizers for reference. The detuning is measured from  $F = 1 \rightarrow F' = 1$  transition on the D1 line of  $^{87}\text{Rb}$ .

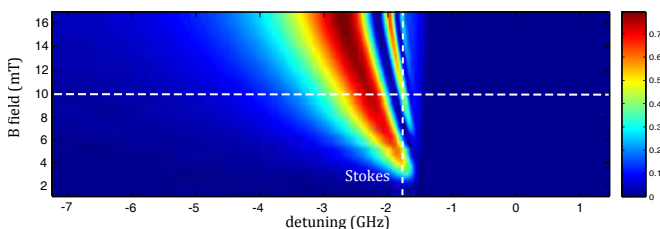


Figure 10. Transmission spectra of both filters for different magnetic fields inside the Faraday filter. The detuning is measured from  $F = 2 \rightarrow F' = 2$  transition on the D1-line of  $^{87}\text{Rb}$ . Temperatures of the filters were  $T_{\text{abs}} = 100^\circ \text{C}$  and  $T_{\text{Farad}} = 102^\circ \text{C}$ , respectively for the absorption and Faraday filter.

### C. Transmission of combined filters

The transmission through both filters for the D1 line Rubidium spectrum is depicted in Fig. 10. Both filters transmit light at the frequencies detuned to the red from the  $F = 2 \rightarrow F' = 2$  resonant transition. The frequency corresponding to the maximum transmission can be adjusted by proper settings of the Faraday filter's temperature and the internal magnetic field. For positive detunings we observe a sharp edge of absorption region resulting from the presence of the absorption filter.

We found the optimal conditions for the operation of the filtering system to be:  $T_{\text{abs}} = 100^\circ \text{C}$  and  $T_{\text{Farad}} = 102^\circ \text{C}$ , with the magnetic field amplitude inside the Faraday filter  $B = 10^{-2} \text{T}$ . For such settings the combined transmission through absorption and Faraday filters is depicted in Fig. 3. Remarkably for Raman-scattered light detuned from the  $F = 2 \rightarrow F' = 2$  resonant transition by  $\Delta_S = -2.3 \text{GHz}$  and  $\Delta_{AS} = 7.8 \text{GHz}$  we achieved a high transmission of 65% and 40% for Stokes and anti-Stokes light respectively.

## IV. PERFORMANCE - FILTERING PHOTONS FROM THE MEMORY

To qualitatively assess the performance of the filtering system, we measured Stokes photons along with subsequently retrieved anti-Stokes photons in a similar manner as [20], but in a low gain regime exciting only a few photons per spatial mode [39]. We observe an increase in the signal-to-noise ratio owing to the filtering system by measuring average intensities and correlations between the number of photons generated in the write-in and readout process.

The average intensities from  $2 \times 10^5$  frames registered on the I-sCMOS camera are depicted in Fig. 11. The first line presents the angularly broad Stokes and anti-Stokes light intensities without the Faraday filter, while the second one includes Faraday filter operation where the isotropic noise background is greatly suppressed. For comparison the residual laser beams (angularly narrow) leakage is let through the filters in the system by with cold  $^{85}\text{Rb}$  filter, as depicted in the third line.

The joint statistics  $p(n_S, n_{AS})$  of counts between Stokes and anti-Stokes photons from the write-in and readout processes are depicted in Fig. 12 (a) and (b), with and without the Faraday filter, respectively. We count the number of Stokes photons  $n_S$  scattered on the camera region around the write-in laser beam (6 mrad in diameter) and the number of anti-Stokes photons  $n_{AS}$  around the readout beam.

Comparing the maps of the joint statistics, one can see that application of the Faraday filter enables observation of a correlation between the amount of Stokes and anti-Stokes photons scattered in each realization of the experiment. The ratio of the size of the diagonal and anti-diagonal joint probability distribution is a measure of correlation coefficient and thus the signal-to-noise ratio in the registered data. Without the Faraday filter the number of anti-Stokes scattered photons is almost independent of the number of Stokes-scattered photons. This is due to spurious incoherent light which is intense enough to cover the Raman scattering signal.

To demonstrate the multimode capacity of our memory and filter system we conduct direction-resolved measurements of correlations. To this end we divide the camera region along the horizontal line to the left and right around the write and read beams into small circular regions  $A_i$  and  $A_j$ , each of the area of  $0.02 \text{mrad}^2$  and with 0.7-0.8 single photon on average. We calculated the correlation coefficient  $C_{ij} = \langle \Delta n_S(A_i) \Delta n_{AS}(A_j) \rangle / \sqrt{\langle (\Delta n_S(A_i))^2 \rangle \langle (\Delta n_{AS}(A_j))^2 \rangle}$  between the number of Stokes  $n_S(A_i)$  and anti-Stokes  $n_{AS}(A_j)$  photons scattered in the circular regions  $A_i, A_j$  around the write and read beam, respectively. The maps of correlation coefficient between number of the Stokes and anti-Stokes photons scattered into each pair of circular regions are depicted in Figs. 12(c) and (d).

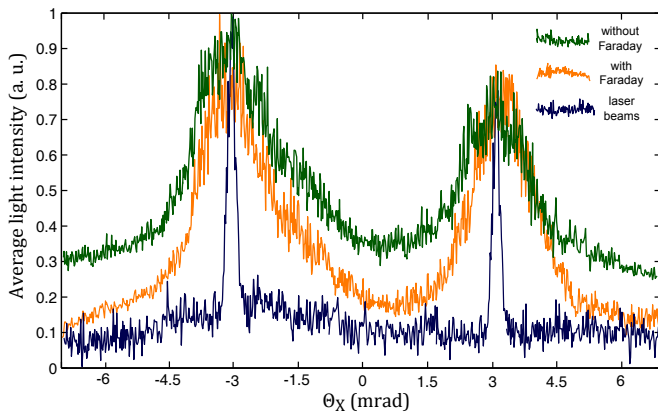


Figure 11. Normalized average light intensities of angularly broad Stokes (left) and anti-Stokes (right) scattering registered by the I-sCMOS camera along the  $\theta_X$  axis. Application of the Faraday filter considerably diminishes the isotropic fluorescence background. Raman scattering is compared with angularly narrow laser beam leakage which dominates without absorption filter.

Using Faraday filter the four-wave-mixing contribution [50] has been eliminated.

Then we compare the number of coincidences of Stokes and anti-Stokes photons from each of these small regions. Including the Faraday filter we are able to observe the elliptic structure which is evidence for generation of correlated photon pairs with a correlation coefficient of 0.38 which is smaller than unity because of the fluorescence signal from the quantum memory cell.

Without the narrowband Faraday filter we do not observe any correlations on the illumination level of  $\bar{n} = 30$  photons per camera frame (from which  $\bar{n}_b = 1.5$  is the light-independent equivalent background illumination noise of the image intensifier). The correlation coefficient between the Stokes and anti-Stokes photons scattered in the opposite directions extracted from the measured data is as little as ca. 0.03 on average which is negligible as compared to Fig. 12(c) with Faraday filter. Moreover, in Fig. 12(d) there is no visible structure, which is due to the large amount of fluorescence light comparable to the Raman-scattered photons which are correlated.

## V. CONCLUSIONS

In conclusion we built and characterized a two-step filtering setup which enables observation of the correlations between Stokes and anti-Stokes Raman scattering at a single-photon-level.

Polarization pre-filtering and a rubidium absorption filter are used to eliminate the laser beams leakage by attenuating them by more than  $10^9$ , while an additional combination with a Faraday filter yields a total attenua-

tion of  $10^{11}$ .

Moreover the Faraday filter blocks the fluorescence and the four-wave-mixing noise coming from the atomic memory medium. The filter transmits only the narrowband spectrum of frequencies corresponding to the Raman-scattered light in  $^{87}\text{Rb}$ . In the case of our filter construction it corresponds to the frequencies detuned approximately by  $\Delta_S = -2$  GHz and  $\Delta_{AS} = 7$  GHz from the  $F = 2 \rightarrow F' = 2$  resonant transition for Stokes and anti-Stokes light, respectively. Noticeably, regardless of such small detunings we achieve a transmission for the Raman-scattered light as high as 50-60%, depending on the Faraday filter settings.

Our approach is robust and efficient. Which is more, the frequencies with high transmission can be tuned by several hundreds of MHz by changing the magnetic field amplitude inside the Faraday filter, whereas absorption edges of  $^{85}\text{Rb}$  filter can be moved magnetically as widely as up to 8.4 GHz. Eventually we can obtain the optimal, high transmission on the Raman-scattered light frequencies while blocking frequencies corresponding to the broadband fluorescence, laser beams and four-wave-mixing.

The performance of the system in the regime of a few atomic collective excitations is evaluated in statistical measurements of the scattered photons. The obtained correlation maps are strong evidence for the directional coincidences between Raman-scattered light produced in the write-in and readout processes of quantum memory. However, the output signal is dominated by noise and no correlation appears above the background if no filtering is applied.

Nowadays, many groups are utilizing warm atomic and

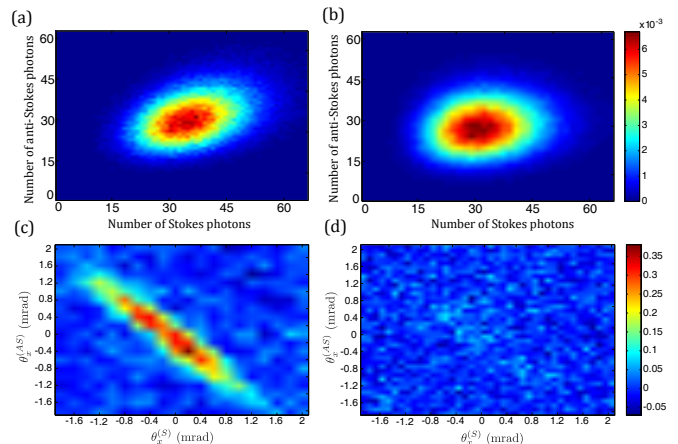


Figure 12. Comparison of measured joint photon statistics (a-b) and spatial correlations between the Stokes and anti-Stokes photons (c-d) with (left panel) and without (right panel) Faraday filter. The joint count statistics of centrally emitted Stokes and anti-Stokes (top row)  $p(n_S, n_{AS})$  and maps of intensity correlations between different directions (bottom row).

molecular gases for quantum memories [1, 4, 12, 13, 18–24, 38, 40–42, 57–61]. Application of the filtering system we present can enhance the fidelity of retrieved photons and extend other teams’ operational regime into the multimode quantum memory [37, 61]. Undoubtedly such system will be essential to measure non-classical  $g^{(2)}$  cross-correlation function between stored and retrieved photons [6, 21, 62], which is prerequisite for further applications in quantum information processing. Importantly presented filtering solution can find applications far beyond quantum memories including Raman spectroscopy [63] and biological applications [64].

## ACKNOWLEDGMENTS

We acknowledge discussions with Michał Parniak, Czesław Radzewicz and Cezary Samojłowicz, generous support of Konrad Banaszek, as well as technical support of Jarosław Iwaszkiewicz, Marcin Piasecki and Szymon Żuchowski.

## FUNDING

This project was financed by the National Science Centre No. DEC-2011/03/D/ST2/01941 and DEC-2013/09/N/ST2/ 02229 and PhoQuS@UW (Grant Agreement no. 316244) co-financed by the Polish Ministry of Science and Higher Education. R.C. was supported by Foundation for Polish Science (FNP).

---

\* radekch@fuw.edu.pl

- [1] Bussi eres, F.; Sangouard, N.; Afzelius, M.; de Riedmatten, H.; Simon, C.; et al. *J. Mod. Opt.* **2013**, *60* (18), 1519–1537.
- [2] Kimble, H.J. *Nature* **2008**, *453* (7198), 1023–1030.
- [3] Lee, K.C.; Sussman, B.J.; Sprague, M.R.; Michelberger, P.; Reim, K.F.; Nunn, J.; Langford, N.K.; Bustard, P.J.; Jaksch, D.; Walmsley, I.A. *Nat. Photonics* **2011**, *6* (1), 41–44.
- [4] Bustard, P.J.; Lausten, R.; England, D.G.; Sussman, B.J. *Phys. Rev. Lett.* **2013**, *111* (8), 083901.
- [5] Kuzmich, A.; Bowen, W.P.; Boozer, A.D.; Boca, A.; Chou, C.W.; Duan, L.-M.; Kimble, H.J. *Nature* **2003**, *423* (6941), 731–734.
- [6] Lee, K.C.; Sprague, M.R.; Sussman, B.J.; Nunn, J.; Langford, N.K.; Jin, X.M.; Champion, T.; Michelberger, P.; Reim, K.F.; England, D.; Jaksch, D.; Walmsley, I.A. *Science* **2011**, *334* (6060), 1253–1256.
- [7] Nunn, J.; Langford, N.; Kolthammer, W.; Champion, T.; Sprague, M.; Michelberger, P.; Jin, X.M.; England, D.; Walmsley, I.A. *Phys. Rev. Lett.* **2013**, *110* (13), 133601.
- [8] Veissier, L.; Nicolas, A.; Giner, L.; Maxein, D.; Sheremet, A.S.; Giacobino, E.; Laurat, J. *Opt. Lett.* **2013**, *38* (5), 712–714.
- [9] Reim, K.F.; Nunn, J.; Lorenz, V.O.; Sussman, B.J.; Lee, K.C.; Langford, N.K.; Jaksch, D.; Walmsley, I.A. *Nat. Photonics* **2010**, *4* (4), 218–221.
- [10] Hedges, M.P.; Longdell, J.J.; Li, Y.; Sellars, M.J. *Nature* **2010**, *465* (7301), 1052–1056.
- [11] Clausen, C.; Usmani, I.; Bussi eres, F.; Sangouard, N.; Afzelius, M.; de Riedmatten, H.; Gisin, N. *Nature* **2011**, *469* (7331), 508–511.
- [12] Hosseini, M.; Sparkes, B.M.; H etet, G.; Longdell, J.J.; Lam, P.K.; Buchler, B.C. *Nature* **2009**, *461* (7261), 241–245.
- [13] de Almeida, A.J.F.; Barreiro, S.; Martins, W.S.; de Oliveira, R.A.; Felinto, D.; Pruvost, L.; Tabosa, J.W.R. *Opt. Lett.* **2015**, *40* (11), 2545–2548.
- [14] Radnaev, A.G.; Dudin, Y.O.; Zhao, R.; Jen, H.H.; Jenkins, S.D.; Kuzmich, A.; Kennedy, T.A.B. *Nat. Phys.* **2010**, *6* (11), 894–899.
- [15] Choi, K.S.; Goban, A.; Papp, S.B.; van Enk, S.J.; Kimble, H.J. *Nature* **2010**, *468* (7322), 412–416.
- [16] Bao, X.H.; Reingruber, A.; Dietrich, P.; Rui, J.; D uck, A.; Strassel, T.; Li, L.; Liu, N.L.; Zhao, B.; Pan, J.-W. *Nat. Phys.* **2012**, *8* (7), 517–521.
- [17] Stack, D.T.; Lee, P.J.; Quraishi, Q. *Opt. Express* **2015**, *23* (5), 6822–6832.
- [18] van der Wal, C.H.; Eisaman, M.D.; Andre, A.; Walsworth, R.L.; Phillips, D.F.; Zibrov, A.S.; Lukin, M.D. *Science* **2003**, *301*, 196–200.
- [19] Hosseini, M.; Campbell, G.; Sparkes, B.M.; Lam, P.K.; Buchler, B.C. *Nat. Phys.* **2011**, *7* (10), 794–798.
- [20] Chrapkiewicz, R.; Wasilewski, W. *Opt. Express* **2012**, *20* (28), 29540–29551.
- [21] Bashkansky, M.; Fatemi, F.K.; Vurgafman, I. *Opt. Lett.* **2012**, *37* (2), 142–144.
- [22] Sprague, M.R.; England, D.G.; Abdolvand, A.; Nunn, J.; Jin, X.M.; Steven Kolthammer, W.; Barbieri, M.; Rigal, B.; Michelberger, P.S.; Champion, T.F.M.; Russell, P.S.J.; Walmsley, I.A. *New J. Phys.* **2013**, *15* (5), 055013.
- [23] Sprague, M.R.; Michelberger, P.S.; Champion, T.F.M.; England, D.G.; Nunn, J.; Jin, X.M.; Kolthammer, W.S.; Abdolvand, A.; Russell, P.S.J.; Walmsley, I.A. *Nat. Photonics* **2014**, *8* (4), 287–291.
- [24] Bustard, P.J.; Erskine, J.; England, D.G.; Nunn, J.; Hockett, P.; Lausten, R.; Spanner, M.; Sussman, B.J. *Opt. Lett.* **2015**, *40* (6), 922–925.
- [25] Maurer, P.C.; Kucsko, G.; Latta, C.; Jiang, L.; Yao, N.Y.; Bennett, S.D.; Pastawski, F.; Hunger, D.; Chisholm, N.; Markham, M.; Twitchen, D.J.; Cirac, J.I.; Lukin, M.D. *Science* **2012**, *336* (6086), 1283–1286.
- [26] de Riedmatten, H.; Afzelius, M.; Staudt, M.U.; Simon, C.; Gisin, N. *Nature* **2008**, *456* (7223), 773–777.
- [27] Saglamyurek, E.; Sinclair, N.; Jin, J.; Slater, J.A.; Oblak, D.; Bussi eres, F.; George, M.; Ricken, R.; Sohler, W.; Tittel, W. *Nature* **2011**, *469* (7331), 512–515.
- [28] Parniak, M.; Wasilewski, W. *Appl. Phys. B* **2013**, *116* (2), 415–421.
- [29] Chrapkiewicz, R.; Wasilewski, W.; Radzewicz, C. *Opt. Commun.* **2014**, *317*, 1–6.
- [30] Kołodyński, J.; Chwedeńczuk, J.; Wasilewski, W. *Phys. Rev. A* **2012**, *86* (1), 013818.
- [31] Dąbrowski, M.; Parniak, M.; Pecak, D.; Chrapkiewicz, R.; et al. *Latvian Journal of Physics and Technical Sciences* **2014**, *51* (5), 21–34.
- [32] Parniak, M.; Wasilewski, W. *Phys. Rev. A* **2015**, *91* (2), 023418.

- [33] Parniak, M.; Pećak, D.; Wasilewski, W. *Pre-print arXiv: arXiv:1505.04118* **2015**, arXiv.org e-Print archive. <http://arxiv.org/abs/1505.04118>.
- [34] Chrapkiewicz, R.; Wasilewski, W. *J. Mod. Opt.* **2010**, *57* (5), 345–355.
- [35] Boyer, V.; Marino, A.M.; Pooser, R.C.; Lett, P.D. *Science* **2008**, *321* (5888), 544–547.
- [36] Boyer, V.; Marino, A.; Lett, P.D. *Phys. Rev. Lett.* **2008**, *100* (14), 143601.
- [37] Surmacz, K.; Nunn, J.; Reim, K.; Lee, K.C.; Lorenz, V.O.; Sussman, B.J.; Walmsley, I.A.; Jaksch, D. *Phys. Rev. A* **2008**, *78* (3), 033806.
- [38] Glorieux, Q.; Clark, J.B.; Marino, A.M.; Zhou, Z.; Lett, P.D. *Opt. Express* **2012**, *20* (11), 12350.
- [39] Chrapkiewicz, R.; Dąbrowski, M.; Wasilewski, W. *CLEO: 2015 Postdeadline Paper Digest*, paper JTh5B.8, DOI: 10.1364/CLEO\_AT.2015.JTh5B.8.
- [40] Heifetz, A.; Agarwal, A.; Cardoso, G.C.; Gopal, V.; Kumar, P.; Shahriar, M.S. *Opt. Commun.* **2004**, *232* (1-6), 289–293.
- [41] Eisaman, M.; Childress, L.; André, A.; Massou, F.; Zibrov, A.; Lukin, M.D. *Phys. Rev. Lett.* **2004**, *93* (23), 233602.
- [42] Manz, S.; Fernholz, T.; Schmiedmayer, J.; Pan, J-W. *Phys. Rev. A* **2007**, *75* (4), 040101(R).
- [43] Shen, Y.R. *Phys. Rev. B* **1974**, *9* (2), 622–626.
- [44] Rousseau, D.L.; Patterson, G.D.; Williams, P.F. *Phys. Rev. Lett.* **1975**, *34* (21), 1306–1309.
- [45] Raymer, M.G.; Carlsten, J.L. *Phys. Rev. Lett.* **1977**, *39* (21), 1326–1329.
- [46] Childress, L.; Taylor, J.M.; Sørensen, A.S.; Lukin, M.D. *Phys. Rev. A* **2005**, *72* (5), 052330.
- [47] Hedges, R.E.M.; Drummond, D.L.; Gallagher, A. *Phys. Rev. A* **1972**, *6* (4), 1519–1544.
- [48] Zielinska, J.A.; Beduini, F.A.; Godbout, N.; Mitchell, M.W. *Opt. Lett.* **2012**, *37* (4), 524–526.
- [49] Zielinska, J.A.; Beduini, F.A.; Lucivero, V.G.; Mitchell, M.W. *Opt. Express* **2014**, *22* (21), 25307–25317.
- [50] Dąbrowski, M.; Chrapkiewicz, R.; Wasilewski, W. *Opt. Express* **2014**, *22* (21), 26076–26090.
- [51] Chrapkiewicz, R.; Wasilewski, W.; Banaszek, K. *Opt. Lett.* **2014**, *39* (17), 5090.
- [52] Jachura, M.; Chrapkiewicz, R. *Opt. Lett.* **2015**, *40* (7), 1540–1543.
- [53] Jachura, M.; Chrapkiewicz, R.; Demkowicz-Dobrzański, R.; Wasilewski, W.; Banaszek, K. *arXiv:1504.05435* **2015**, arXiv.org e-Print archive. <http://arxiv.org/abs/1504.05435>.
- [54] Chrapkiewicz, R. *J. Opt. Soc. Am. B* **2014**, *31* (10), B8.
- [55] Chrapkiewicz, R.; Jachura, M.; Banaszek, K.; Wasilewski, W. *arXiv:1509.02890* **2015**, arXiv.org e-Print archive. <http://arxiv.org/abs/1509.02890>.
- [56] Kiefer, W.; Löw, R.; Wrachtrup, J.; Gerhardt, I. *Sci. Rep.* **2014**, *4*, 6552.
- [57] Eisaman, M.D.; André, A.; Massou, F.; Fleischhauer, M.; Zibrov, A.S.; Lukin, M.D. *Nature* **2005**, *438* (7069), 837–41.
- [58] Jiang, W.; Han, C.; Xue, P.; Duan, L.M.; Guo, G-C. *Phys. Rev. A* **2004**, *69* (4), 043819.
- [59] Michelberger, P.S.; Champion, T.F.M.; Sprague, M.R.; Kaczmarek, K.T.; Barbieri, M.; Jin, X.M.; England, D.G.; Kolthammer, W.S.; Saunders, D.J.; Nunn, J.; Walmsley, I.A. **2014**, *174* (2007), 285–291.
- [60] Lvovsky, A.I.; Sanders, B.C.; Tittel, W. *Nat. Photonics* **2009**, *3* (12), 706–714.
- [61] Nunn, J.; Reim, K.; Lee, K.C.; Lorenz, V.O.; Sussman, B.J.; Walmsley, I.A.; Jaksch, D. *Phys. Rev. Lett.* **2008**, *101* (26), 260502.
- [62] Kasperczyk, M.; Jorio, A.; Neu, E.; Maletinsky, P.; Novotny, L. *Opt. Lett.* **2015**, *40* (10), 2393.
- [63] Lin, J.; Li, Y-Q. *Opt. Lett.* **2014**, *39* (1), 108–110.
- [64] Uhlend, D.; Rendler, T.; Widmann, M.; Lee, S.Y.; Wrachtrup, J.; Gerhardt, I. *arXiv:1502.07568* **2015**, arXiv.org e-Print archive. <http://arxiv.org/abs/1502.07568>.